6458–6470 *Nucleic Acids Research, 2020, Vol. 48, No. 12* *Published online 4 June 2020*
doi: 10.1093/nar/gkaa479

Dynamic topology of double-stranded telomeric DNA studied by single-molecule manipulation *in vitro*

Xiaonong Zhang, Yingqi Zhang and Wenke Zhang *

State Key Laboratory of Supramolecular Structure and Materials, Jilin University, Changchun 130012, People's Republic of China

Received December 18, 2019; Revised May 17, 2020; Editorial Decision May 25, 2020; Accepted May 27, 2020

ABSTRACT

The dynamic topological structure of telomeric DNA is closely related to its biological function; however, no such structural information on full-length telomeric DNA has been reported due to difficulties synthesizing long double-stranded telomeric DNA. Herein, we developed an EM-PCR and TA cloning-based approach to synthesize long-chain double-stranded tandem repeats of telomeric DNA. Using mechanical manipulation assays based on single-molecule atomic force microscopy, we found that mechanical force can trigger the melting of double-stranded telomeric DNA and the formation of higher-order structures (G-quadruplexes or i-motifs). Our results show that only when both the G-strand and C-strand of double-stranded telomeric DNA form higher-order structures (G-quadruplexes or i-motifs) at the same time (e.g. in the presence of 100 mM KCl under pH 4.7), that the higher-order structure(s) can remain after the external force is removed. The presence of monovalent K^+, single-wall carbon nanotubes (SWCNTs), acidic conditions, or short G-rich fragments (∼30 nt) can shift the transition from ds-DNA to higher-order structures. Our results provide a new way to regulate the topology of telomeric DNA.

INTRODUCTION

Telomeres are eukaryotic linear chromosomal protection ends, and telomere shortening is a factor that causes cell senescence (1). They are also critical for genomic integrity and play an important role in cancer (2). The function of telomeres is closely related to their structural specificity. In mammals, telomeric DNA is composed of thousands of $(TTAGGG)_n/(CCCTAA)_n$ repeats (3), and the G-rich strand forms a short (∼50–400 nt) single-stranded overhang on the 3′ end (4–6), which can invade into upstream duplex telomeric DNA resulting in a telomere loop (t-loop) (7–9). At the same time, both G-rich and C-rich strands can form unusual higher-order DNA structures. G-rich DNA can fold into DNA G-quadruplexes consisting of tetrameric guanine residues arranged in quadrilateral planes (10). The G-quadruplexes formed by a 3′ overhang can inhibit telomerase activity (11–13), and the G-quadruplexes formed on the double-stranded telomeric sequence play an important role in regulating DNA replication, transcription, and translation (14–16). The C-rich regions can form another tetraplex structure, i.e. the so-called i-motif, with a stack of hemiprotonated cytosine–cytosine ($C{\cdot}C^+$) pairs (17–19). These are usually stabilized under acidic conditions (20). Molecular crowding (21,22) and negative superhelicity (23) induced during transcription can help i-motifs form at physiological pH. The i-motif has been identified in telomeres, centromeres, and some oncogene promoter regions (24,25); it also has biological roles in modulating replication and transcription (26–31).

The structural polymorphisms of telomeric DNA *in vivo* are of great scientific interest in drug design and chemotherapy. Higher-order structures (i-motifs or G-quadruplexes) and Watson-Crick duplex competition have been studied since the 1990s (32–34). NMR, UV spectroscopy, and circular dichroism (CD) have demonstrated that under near physiological conditions of pH, temperature, and salt concentration, telomeric DNA tends to exist in a double-stranded form. However, the G-quadruplex or i-motif structure will appear at higher temperatures or lower pH values (35–37). In addition, the duplex can be inhibited by negative superhelicity (23), molecule crowding (38), and the small molecules that stabilize the G-quadruplex (37) or i-motif DNA (39). The G-quadruplex and i-motif in the promoter region can co-exist at the single molecule level (40–42). However, research objects in these studies are short DNA chains, which cannot fully reflect the real situation of telomeric sequences at the end of the chromosome (composed of thousands of the $(TTAGGG)_n/(CCCTAA)_n$ repeats). Therefore, the dynamic topological structure of long-chain double-stranded telomeric DNA must be explored.

Panczyk *et al.* recently used molecular dynamics simulation to show that a decrease in pH causes protonation of ruthenium to form C^+G. This will reduce the hydrogen bonds between the C–G pairs and slowly destroy the structure of the double-stranded DNA. This can result in the

*To whom correspondence should be addressed. Tel: +86 431 85159203; Fax: +86 431 85159203; Email: zhangwk@jlu.edu.cn

formation of the i-motif structure (43,44). Thus, the stability of the hydrogen bonds between the helix is an important factor determining the telomere DNA topology. The G-quadruplex formation in telomeric duplex is correlated with DNA melting (45). Mechanical forces govern numerous biological processes (46–49). *In vivo*, mechanical force is another important factor that can affect the stability of ds-DNA and induce DNA melting. The mechanical stability of individual DNA molecules has been an important scientific issue for decades (50–53). However, there have been few breakthroughs on the influence of mechanical force on the topology of long-chain telomeric DNA.

Due to the rapid reannealing and low selectivity of repetitive sequences, it is difficult to synthesize double-stranded telomeric DNA *in vitro*. This is an important factor hindering the development of this field. For double-stranded repeat sequences, the usual preparation methods are the slippage reaction (54–56) or an enzymatic method based on the polymerase chain reaction (EM-PCR) (57). While these two methods have some problems, the product obtained by the slippage reaction is noticeably short while the latter produces a broad distribution of DNA molecular weights. Although gel purification was used to enrich the DNA, no marked improvements were seen (57). The sample cannot be amplified by PCR due to the repeating sequence (58). Therefore, it is critical to find a way to synthesize the long-chain double-stranded telomeric DNA.

In this article, we combined EM-PCR and TA cloning approaches to solve the problem of synthesizing double-stranded telomeric DNA *in vitro*. The properties of telomere DNA were studied by AFM-based single molecule force spectroscopy (SMFS). This is a well-developed practical technique used widely in the investigation of mechanical properties of DNA and its higher-order structures (36,42,45,50,51,59–63). We found that long-chain telomeric DNA predominantly exists as a double helix at either physiological or acidic pH. However, after DNA undergoes force-induced melting, telomere DNA will form different topologies during the renaturation process under different environments. At physiological pH, the renaturation of the two single strands is rapid, and the double helix is the predominant structure. DNA hybridization can be suppressed in the presence of KCl, at acidic pH, or in the presence of SWCNTs. Single-stranded DNA has the opportunity to fold and form G-quadruplexes or i-motifs. Thus, higher-order structures can eventually be detected along the telomeric DNA. When DNA renaturation is further inhibited, the length of the single strands will increase and lead to the formation of partially folded structures. These results indicate that, apart from the molecule crowding (38) and pH (35), *in vivo* mechanical force is another factor that can induce structural polymorphism of telomeric DNA.

MATERIALS AND METHODS

Materials and strains

All chemical reagents were from commercial sources and were of analytical grade. pMD18-T-Vector kit was purchased from TaKaRa Bio Inc.; JM109 competent cells and DNA molecular weight Marker were purchased from Beijing Dingguo Biotechnology Co. Ltd.; EasyPure Quick Gel Extraction Kit, EasyPure HiPure Plasmid MaxiPrep Kit, EasyPure PCR Purification Kit and Taq DNA Polymerase were purchased from TransGen Biotech (Beijing). Restriction enzymes (BspQI, BstAPI) and T4 DNA ligase were purchased from New England Biolabs Inc.; KOD -Plus- was purchased from TOYOBO. DNA oligomers were purchased from Sangon Biotech (Shanghai) Co., Ltd.. TCEP (Tris(2-carboxyethyl) phosphine), MCH (6-mercaptohexan-1-ol), and NHS-biotin ((+)-biotin *N*-hydroxysuccinimide ester) and SWCNT-COOH were purchased from Sigma-Aldrich LLC. Streptavidin was purchased from Promega.

Construction of recombinant plasmids

EM-PCR amplification. 0.15 μM DNA P1 and 0.15 μM DNA P2 (all sequences used in this work are shown in Supplementary Table S1), 1.0 U KOD Plus polymerase, 1× KOD Plus buffer, 1.0 mM $MgSO_4$, and 0.2 mM deoxynucleotide triphosphates (dNTPs) were mixed with a total volume of 50 μl. Thermocycling was carried out using Bio-Rad by the following method:

30 s at 94°C, 15 s at 61°C and 2 min at 68°C.
Product was then purified using an EasyPure PCR Purification Kit.

TA cloning in pMD18-T-Vector. 5 μg PCR product, 1.0 U Taq DNA polymerase, 1× Taq buffer, 2 mM dNTPs were mixed with a total volume of 50 μl. After incubation at 72°C for 30 min, the product was then purified using an EasyPure PCR Purification Kit. Adenine (A) overhangs were added to the 3′-end of the PCR products using Taq DNA polymerase. Above mentioned product was cloned into a pMD18-T-Vector. The plasmid with the $(TTAGGG)_n/(CCCTAA)_n$ insert was then transformed into competent cells (JM109) for amplification. Bacterial cells were collected through centrifugation after overnight shaking in LB growth medium, and the plasmid was extracted with a Maxiprep Kit. The recombinant plasmid named as pUC18-T2AG3 here, was validated by DNA sequencing (Sangon, Shanghai) (as shown in Supplementary Figure S1).

Preparation of DNA constructs

The dsDNA constructs used in SMFS experiment were prepared by ligating three dsDNA segments, as shown in Figure 2A: one biotin-labeled (559 bp, handle I) segment, one middle (∼1200 bp, contained ∼700 bp telomeric dsDNA) segment, and a 14-bp hairpin with a 5T loop internally labeled with a single thiol group (Supplementary Figure S2).

Handle I. To prepare this biotin-labeled segment (∼559 bp), double-stranded DNA fragments (600 bp) were first obtained using PCR amplification with pUC18 plasmid as a template. We designed the primers such that the PCR products contained the restriction sites near the end of the strands, allowing us to remove the digested useless short DNA fragments via the PCR purification kit instead of gel

purification. Each reaction contains 100 μl solution containing forward (pUC18-668) and reverse (pUC18-1027) primers (40 pmol each) (Supplementary Table S1), 2 mM $MgSO_4$, 2 ng pUC18, 2 U KOD polymerase, and 80 nmol dNTPs (20 nmol each) in KOD buffer. After PCR purification, the products then digested by BspQI restriction endonucleases. We prepared a 100 μl reaction mixture containing 5 μg (11 pmol) of the PCR product, and 50 units BspQI in NEB CutSmart buffer [50 mM Potassium acetate, 20 mM Tris-acetate, 10 mM Magnesium acetate, 100 μg/ml BSA (pH 7.9)]. After 15 min digestion at 37°C, a 5′-GCT-3′ overhang was generated. Then the product was incubated with psoralen in UV 365 nm for 30 min at room temperature, resulting in a crosslinked handle I (559 bp).

Middle part. For the middle segment (∼1200 bp) which contains ∼700 bp telomeric dsDNA, we performed the double-digestion with BspQI and BstAPI simultaneously on the recombinant plasmids (pUC18-T2AG3) and generated 5′-AGC-3′ and 5′-ATG-3′ overhangs at each end. To do that, the 100 μl reaction mixture contained 10 μg of the recombinant plasmids and 50 units BspQI in NEB CutSmart buffer was incubated at 50°C for 20 min, 80°C for 20 min. Then added 100 units BstAPI and incubated at 60°C for 1 h, 80°C for 20 min. The non-palindromic overhangs enhanced the efficiency of the three segments hybridization/ligation reaction.

Handle II. Handle II is a DNA hairpin consists of a TT/HS-T/TT loop capping a 14-base-pair stem that was terminated with a three-base overhang at its 3′-end (as shown in Supplementary Figure S2). To increase the hairpin formation via self-annealing of the oligomer, the DNA solution was heated up to 95°C then slowly cooled to room temperature (about 2 h) prior to ligation.

All the three DNA fragments (Handle I, Middle part and Handle II) were ligated with T4 DNA ligase. The reaction was incubated for 12 h at 16°C. The final product was analyzed by 1% agarose gel and the regions corresponding to DNA of ∼1773 bp (559 + 1200 + 14) were extracted from the gel. The current design of DNA construct is designed to prevent the DNA peeling after force-induced melting.

To prepare the control construct, we crosslinked the middle part with psoralen at UV 365 nm for 30 min. As a result, the force-induced melting and strand separation in telomeric sequences can be inhibited greatly.

Single molecule force spectroscopy

AFM-based SMFS experiments on single telomeric DNA molecule were carried out on a ForceRobot 300 (JPK Instrument AG, Berlin, Germany) in contact mode. Operating details for AFM-based SMFS has been described in previous work (64–68). Spring constant of AFM tips (MSCT, Bruker Nano, Santa Barbara, CA, USA) was calibrated by thermal noise method, and the measured values were between 0.02 and 0.03 N/m. Au substrates were cleaned with piranha solution (70% H_2SO_4 –30% H_2O_2 in volume). The streptavidin modified AFM tips were prepared by following the previously established procedure (65,66). In brief, AFM tips were functionalized first by amino-silanization followed by incubating in NHS-biotin (2 mM) solution for 2 h and then in streptavidin (1 mg/ml) aqueous solution for 10 min.

For the single-time stretching experiment, the tip was brought to contact with the substrate at a contact force of 0.2 nN for 1 s, then stretched at the pulling speed of 1 μm/s.

Circular dichroism (CD) measurement

Using 21mer-C and 21mer-G as primers (see Supplementary Table S1), double-stranded telomeric DNA samples with different length were synthesized by different number of EM-PCR cycles (0, 1, 3, 5× cycle). Recombinant plasmid pUC18-T2AG3 was digested with EcoRI and HindIII (see Figure 1A) to obtain ∼700-bp telomeric dsDNA. For CD measurement, corresponding DNA samples were diluted with 100 mM KCl at pH 7.4 or pH 4.7 to a final concentration of 2–5 μM. The sample was transferred into a 0.2 mm path length quartz cell followed by CD spectra measurements with a MOS-450 spectrometer (Bio-logic, France). All data were collected from 220 to 340 nm with a scan rate of 0.5 nm/s.

UV-melting measurement

700-bp telomeric dsDNA was diluted with 100 mM KCl (pH 4.7) to a final concentration 2 μM. The sample was placed in a 0.5 cm path length quartz cell and loaded onto a UV 2450 spectrometer (Shimadzu, Japan). The measurements were carried out at 295 nm, with a temperature range between 10 and 80°C at a heating rate of 0.5°C/min.

Data analysis

All of AFM data were analyzed using custom software written in Igor Pro (Wavemetrics). The histograms of plateau forces were fitted by using the Gaussian function to obtain the most probable value.

RESULTS AND DISCUSSION

Synthesis of long double-stranded telomeric DNA

The PCR (EM-PCR) used in this work differs from traditional PCR in that the two DNA fragments in this system act as templates and primers at the same time. Heating denatures the duplex, and cooling allows for re-hybridization. The DNA extends along the 3′ end of the primer with the help of the KOD polymerase. Only dsDNA with broad molecular weight distributions can be obtained with this method, and it is difficult to obtain the DNA sample with an accurate length despite Pike *et al.* establishing a method to calculate the maximum and minimum values for the length of the product (57).

Here, we first chose $(TTAGGG)_5$ and $(CCCTAA)_5$ as primers to synthesize telomeric sequences with a dispersive length as shown in Figure 1B. As the number of reaction cycles increases, the molecular weight of the product increases accordingly. The length of telomeric DNA obtained by 14 cycles (lane 4) is moderate, and thus it was selected as the starting materials for the next step. A base 'A' was added to the 3′ end of the PCR product by Taq DNA polymerase.

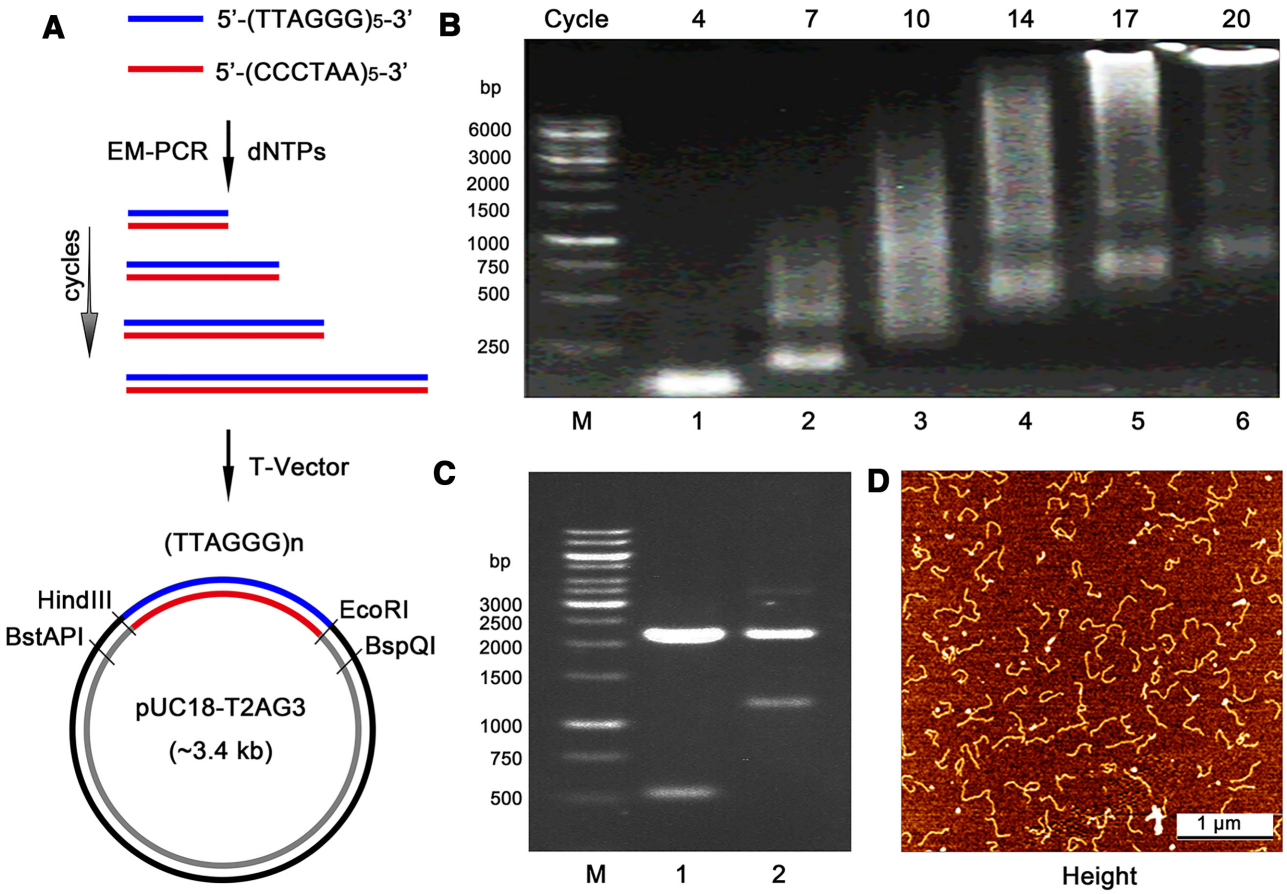

Figure 1. (**A**) Schematics of the construction of the recombinant plasmid. Short $(TTAGGG)_5$ (blue fragment) and $(CCCTAA)_5$ (red fragment) DNAs were extended by EM-PCR and then inserted into the T-Vector. The recombinant plasmid that contains double-stranded telomeric DNA can be obtained after overnight transfection and incubation. (**B**) Agarose gel analysis of the extension products produced from $(TTAGGG)_5$ and $(CCCTAA)_5$ during EM-PCR. Lane 1: 4 cycles; lane 2: 7 cycles; lane 3: 10 cycles; lane 4: 14 cycles; lane 5: 17 cycles; and lane 6: 20 cycles. (**C**) The T-Vector and the recombinant plasmid were double-digested by BspQI and BstAPI restriction endonucleases. The products were analyzed by agarose gel as shown in lane 1 (T-Vector) and lane 2 (recombinant, pUC18-T2AG3), respectively. (**D**) AFM imaging of telomeric-sequence-containing DNA (∼1200 bp) on mica.

After purification, the products were ligated with T-Vector, and the ligation product was transformed into JM109 competent cells.

After transfection and overnight incubation, a single colony on the culture plate was selected and cultured. The plasmid was extracted using standard protocols and digested with corresponding restriction enzymes (BspQI and BstAPI). For comparison, the T-Vector without the insertion was also similarly processed. Figure 1C shows that the cyclized T-Vector exhibits two fragments at ∼2200 and ∼500 bp, respectively, after digestion. The digested recombinant plasmid (pUC18-T2AG3) produced two fragments of ∼2200 bp and ∼1200 bp indicating that the length of the inserted telomeric sequence was ∼700 bp. The successful insertion of telomeric DNA was further confirmed by DNA sequencing (Supplementary Figure S1).

The 1200 bp fragment that contained the telomeric sequence was purified by gel extraction and characterized by AFM imaging as shown in Figure 1D. The length of the DNA in the scanning image is about 384±43 nm (Supplementary Figure S3), which is equivalent to ∼1130 bp and is consistent with the agarose gel result of ∼1200 bp.

Long telomeric dsDNA are stable at either physiological or acidic pH

These characterizations prove the successful preparation of the double-stranded DNA (∼1200 bp) containing a ∼700 bp telomeric sequence (colored fragment). To investigate the mechanical properties of such a telomeric DNA using single molecule force spectroscopy, we added two DNA handles to the 1200 bp dsDNA by ligation (Figure 2A). In doing this, a topologically closed but rotationally unconstrained DNA construct containing a biotin group at one end and a thiol group embedded in a 5-nucleotide loop was obtained (Figure 2A) (see the Materials and Methods section and Supplementary Figures S2 and S4 for more details on the construction of the dsDNA).

The DNA construct can then be linked in between the AFM tip and gold substrate by biotin-streptavidin and gold–thiol interactions. Figure 2B is a typical force–extension (*F*–*E*) curve of double-stranded telomeric DNA obtained in 10 mM MES and 100 mM KCl at pH 4.7. This has a well-known and highly cooperative DNA overstretching transition at ∼62 pN (Figure 2B) (50,69). Below 50 pN,

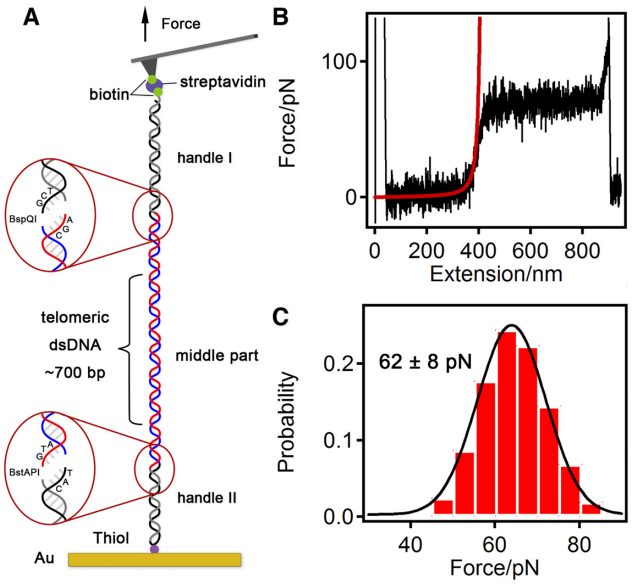

Figure 2. (**A**) Experimental setup for investigating double-stranded telomeric DNA. The DNA molecule is chemically bound to a gold surface (via thiol-gold chemistry) and picked up by an AFM tip through the streptavidin-biotin interactions. (**B**) Typical force-extension curve of telomeric dsDNA in 100 mM KCl, at pH 4.7. The red trace is a WLC fit to the experimental curve with a persistence length of $P = 50$ nm. (**C**) Histogram of transition force ($n = 97$).

the stretching curves nicely fit with the WLC (red line in Figure 2B) model, and the persistence length is ∼50 nm. Similar stretching curves and plateau force were obtained at pH 7.7 and 100 mM KCl (see Supplementary Figure S5 for details). These results indicate that the initial topological structure of telomeric dsDNA is the B-form double-helix regardless of acidic pH or physiological pH. However, previous reports showed that short telomeric sequences (22 nt) exist predominantly as G-quadruplex or i-motif structure instead of duplexes (35). Therefore, the properties of long chain telomeric DNA are quite different from those of short chains.

Mechanical forces trigger the topology change of telomeric DNA

To check the effects of mechanical force on the structure of telomeric dsDNA, we performed repeated stretching-relaxation experiments on the same DNA molecule. Figure 3A shows some typical force curves of telomeric dsDNA obtained by repeatedly manipulating the same DNA molecule in 100 mM KCl (pH 7.7). This facilitates the formation of G-quadruplexes. At neutral pH (7.7), most of the stretching and relaxation curve pairs well with a small number of curves exhibiting hysteresis. At forces ∼65 pN, DNA undergoes a DNA overstretching transition, which leads to an elongated DNA by ∼1.6–1.7-fold. This transition is known to be complex. For typical sequences of DNA, it may involve two distinct types of structural changes. One is strand-separation from the open ends or nicks of DNA, which results in increased entropy. The other is a transition to a new type of DNA, termed S-DNA, in which the two strands remain associated in a highly-ordered manner indicated by reduced entropy compared to B-DNA (70,71). Another distinction between the two types is that the strand-separation transition is hysteretic, and the B-S transition is typically non-hysteretic during stretching and relaxation cycles at typical experimental loading/pulling rates (51,72,73). In our current system, we designed the topologically closed but rotationally free assay by sandwiching telomeric dsDNA between a psoralen crosslinked handle and a 5-nucleotide loop (Figure 2A) to prevent the first type transition. Peeling from one end is prevented by the closed hairpin and from the other end is prevented by a handle crosslinked with psoralen, which is reported to have the ability to crosslink 5′TpA sequences with a 365 nm UV light (74,75). The experimental results show that crosslinking DNA through psoralen can effectively inhibit peeling (see Supplementary Figure S6 for details). According to a previous paper (73), at our experimental pulling rate of 1 μm/s, for typical sequences of DNA, the transition should predominantly be the B-S transition. Additionally, strand separation may also happen inside the DNA (at forces greater than 100 pN (71,76,77). So, we speculate that the hysteresis observed in stretching-relaxation curve #10 may be related to the sequencing specificity of the telomeric dsDNA. When the two strands shift along each other by a repeat unit of (TTAGGG)/(CCCTAA), the majority of the two strands can still hybridize with each other. If they shift relative to each other by one bp, they can also form two GC base pairs every six bps. Therefore, multiple metastable physical organizations of the two strands may exist, decreasing the effective base-pairing energy, which in turn results in a lower force plateau for the internal melting transition. In other words, there might be a co-existing non-hysteretic B-S transition and hysteretic internal melting transition in a similar force range.

However, at a lower pH of 4.7, upon comparing Figure 3B and D, we found that the plateau force value during subsequent stretching is significantly decreased in the presence of 100 mM KCl. The plateau length is shortened, and the probability of hysteresis is greatly increased (from 5% to 65%). We speculate that both the G-quadruplex and the i-motif can form in 100 mM KCl at pH 4.7; thus, when the double-stranded telomeric sequence is melted by external forces, the G-rich strand and C-rich strand both tend to fold into higher-order structures. The possibility of the formation of G-quadruplex and the i-motif by the long telomeric dsDNA was further confirmed by CD measurements and UV-melting experiment (see Supplementary Figures S7 and S8). The results show that the 700-bp telomeric dsDNA can form an i-motif/G-quadruplex structure upon thermal denaturation, which inhibits the reformation of dsDNA.

To prove our hypothesis, we performed the same experiment with psoralen-crosslinked telomeric DNA. Our results show that no plateau force/length changes occur during the repeated stretching and relaxation (Supplementary Figure S6). The strand separation and higher-order structure formation (G-quadruplexes or i-motifs) can be efficiently inhibited because the psoralen molecule can crosslink the TA base pair in the telomeric sequences $((TTAGGG)_n/(CCCTAA)_n)$ (see Supplementary Figure S6). These results show that mechanical forces can cause

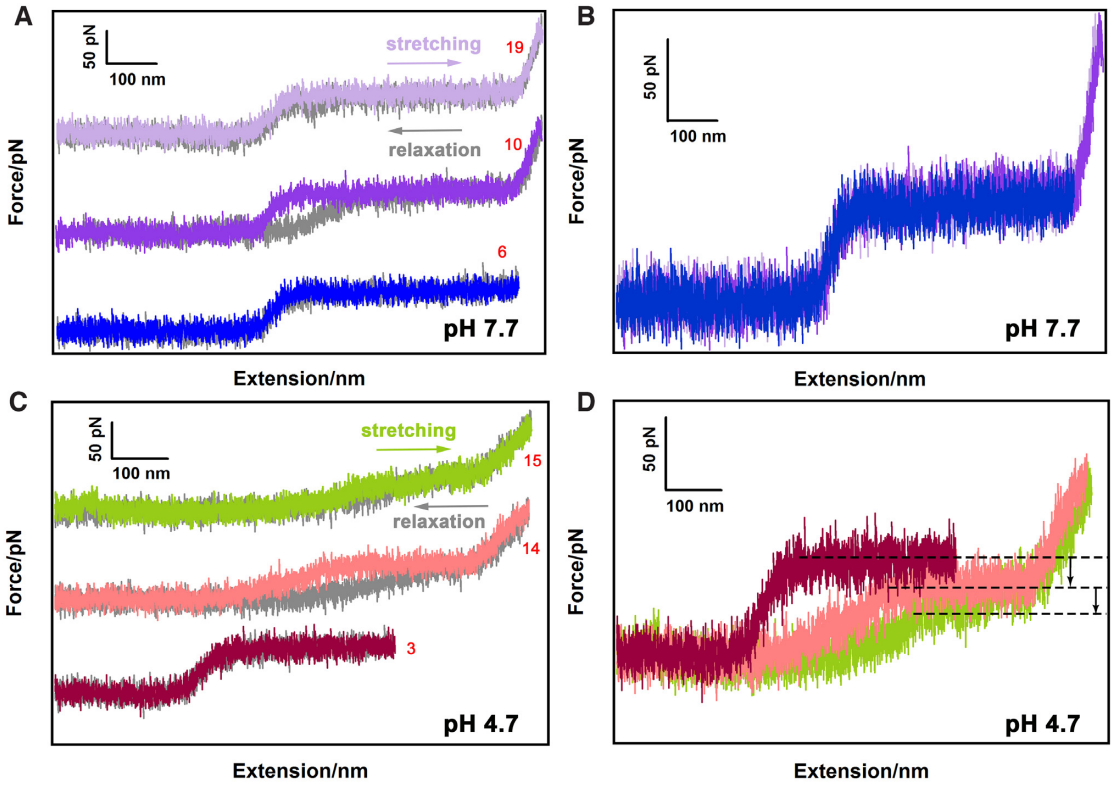

Figure 3. Typical force-extension curves of telomeric dsDNA obtained by repeatedly manipulating the same DNA molecule in: (**A** and **B**) 100 mM KCl, 10 mM Tris–HCl, pH 7.7; (**C** and **D**) 100 mM KCl, 10 mM MES, pH 4.7. Stretching curves obtained at pH 7.7 can be superimposed, and those obtained at pH 4.7 cannot be superimposed. At pH 4.7, the force plateau of the stretching curve is decreased with an increasing number of stretching–relaxation cycles. The curves obtained in different stretching-relaxation cycles are marked in different colors, and the order of the stretching–relaxation cycle is marked numerically.

melting of telomeric dsDNA to facilitate the formation of the G-quadruplex and i-motif structures.

Only both the C-strand and G-strand formed higher-order structures can suppress telomere DNA renaturation

Single-wall carbon nanotubes (SWCNTs) have been reported to be a ligand that can selectively stabilize human telomeric i-motif DNA and can even disrupt short G-rich/C-rich double-stranded associations to induce i-motif formation (39,78). Qu *et al.* (39) proved that SWCNTs can inhibit telomerase activity through stabilization of the i-motif structure. To study the effects of SWCNTs on the structure of long chain telomeric dsDNA, stretching-relaxation experiments were performed in the presence of SWCNT-COOH under different pH values, and the plateau force obtained during cycling was analyzed. Our results show that SWCNTs reduce the plateau force from ∼65 to ∼61 pN at neutral pH and 100 mM KCl for the telomeric dsDNA; the presence of SWCNTs do not cause any obvious changes of the plateau force in the random dsDNA (Figure 4A and B). This phenomenon is because K^+ and SWCNTs facilitate the formation of both G-quadruplex and i-motif after the telomeric dsDNA is melted by external forces. Those higher-order structures can prevent the reannealing of dsDNA during relaxation, causing a reduction of the plateau force. Under acidic conditions (e.g. pH 4.7), the plateau force drops from ∼64 to ∼59 pN in the absence of SWCNTs (Figure 4C). This is because acidic conditions facilitate the formation of an i-motif structure while the presence of K^+ can stabilize the G-quadruplex structure. The introduction of SWCNTs to this system caused a broader distribution of the plateau force in the range of 40–70 pN (Figure 4D). There is another force distribution near 65 pN. The latter may be because of the cumulative stabilization effect of SWCNTs and protons on i-motif structure. A control experiment has also been performed using G-quadruplex-binding ligand (TMPyP4) (79) at pH 4.7 in KCl buffer to elucidate the shift of the equilibrium by formation of G-quadruplex on G-strand (see Supplementary Figure S9).

As a control, we tried the above experiments in the presence of 100 mM LiCl (pH 4.7) (data not shown) in which only the C-strand can fold into i-motifs. The plateau force value of the double-stranded telomeric DNA does not show detectable change during multiple stretching-relaxation cycles. Therefore, we believe that the main reason for the decrease of the plateau force value is as follows: the weak inter-strand interactions (including hydrogen bonding and π–π interactions) between the C-strand and the G-strand are destroyed by the force-induced melting during stretching. The C-strand or G-strand could fold into higher-order structures (i-motifs or G-quadruplexes) in suitable buffer. If only one strand forms higher-order structures, then the re-hybridization of the melted dsDNA can still occur dur-

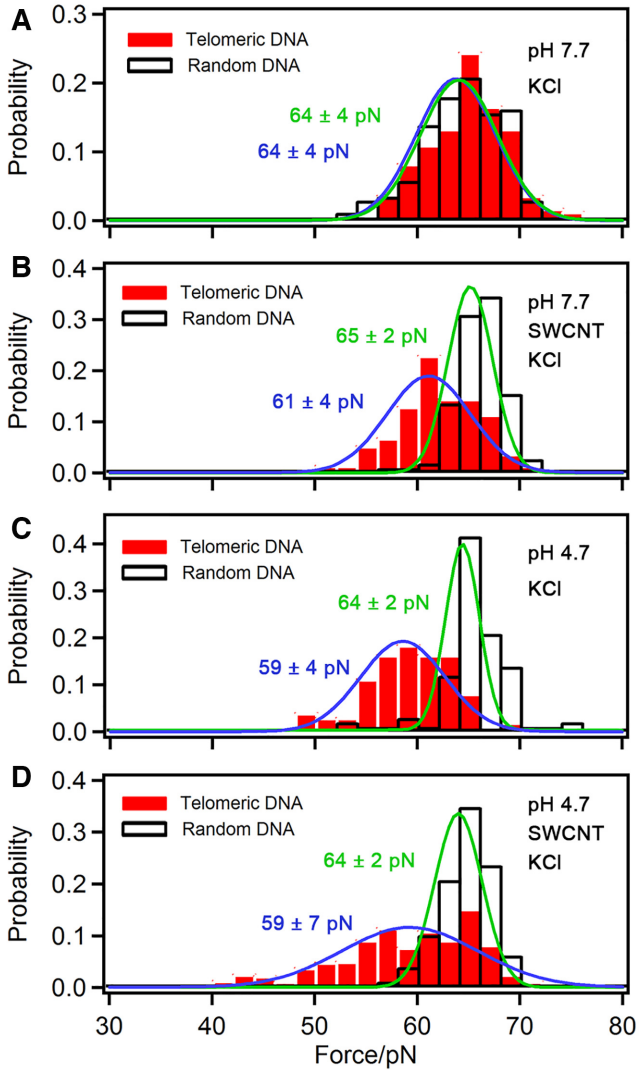

Figure 4. The plateau-force histograms obtained during repeated stretching-relaxation cycles on random DNA (black) and telomeric DNA (red) in different experimental buffer: (**A**) 100 mM KCl, 10 mM Tris, pH 7.7; (**B**) 100 mM KCl, 10 mM Tris, pH 7.7 with 10 μg/ml SWCNT-COOH; (**C**) 100 mM KCl, 10 mM MES, pH 4.7; (**D**) 100 mM KCl, 10 mM MES, pH 4.7 with 10 μg/ml SWCNT-COOH. The Gaussian fittings on the force distributions of telomeric DNA and random DNA are colored in blue and green, respectively. At least 90 single-molecule stretching curves were used for the construction of each of the force histogram.

ing relaxation resulting in the re-appearance of the ∼65 pN force plateau. For example, under pH 7.7 in the presence of 100 mM KCl, the reformation of dsDNA is straightforward (at a stretching speed of 1 μm/s) after the external force is removed since the plateau-containing stretching traces obtained during the subsequent stretching cycles can be superimposed very well (Figure 3B). Under this condition, the G-strand of the telomeric dsDNA has the chance to form G-quadruplex, but it is not stable enough to prevent the reformation of dsDNA although G-quadruplex can occasionally retard the re-hybridization causing hysteresis between the stretching and relaxation traces (see the middle pair of stretching-relaxation traces in Figure 3A). The re-hybridization of the double strand can be suppressed only if both the C- and G-strands form higher-order structures at the same time. For example, at pH 4.7, in the presence of 100 mM KCl, both the G and C-strands have the chance to form a higher-order (G-quadruplex or i-motif) structure at the same time, which will inhibit the reformation of ds-DNA. As shown in Figure 3C, after the strand separation is initiated the original force plateau (at ∼65 pN), which is the force fingerprint of dsDNA (curve #3 in Figure 3C), will not appear during subsequent stretching (curves #14, #15 in Figure 3C) within the time scale of the SMFS experiment (∼5 min). Supplementary Figure S10 shows the time course of the plateau force for five groups of stretching–relaxation data obtained at pH 4.7, in the presence of 100 mM KCl. The lateral axis is the number of stretching-relaxation cycles that the five molecules have undergone, and the vertical axis is the force value of the overstretching plateau under the corresponding cycle. The same conclusion can be drawn from this data: when the buffer conditions facilitate the formation of both G-quadruplex and i-motif the separated G- and C-strands will prevent the reformation of dsDNA efficiently, since the ∼65 pN plateau force cannot be observed again after it is reduced.

Regulation of telomeric DNA topology

Monovalent K^+, pH and SWCNTs can induce single strand G-rich or C-rich folding into higher-order structures and inhibit the reannealing of the double helix. G8A is a DNA fragment of 30 nt in length containing five d(TTAGAG) repeat units (80,81). Here, we used it to complement the vacant C-strand and increase the chances of G-quadruplex formation. In the multiple stretching and relaxation cycles, we observed the appearance of a force curve with two plateaus. A typical double-plateau stretching curve is obtained in 100 mM KCl (pH 4.7) with 10 μg/ml SWCNT (Figure 5A). There is no curve with the double-plateau observed in KCl (pH 7.7) for telomeric DNA (solid triangle). In acidic conditions, pH and SWCNTs are both beneficial to the formation of i-motif structures. The introduction of acid and SWCNTs leads to an increase in the probability of double-plateau and low-force plateau events (Figure 5B). This implies that the formation of both i-motifs and G-quadruplexes explains the double-plateau. Neither of these phenomena appears with random DNA (open circles and triangles).

The plateau-force histogram on double-plateau curves obtained in six different conditions is shown in Figure 5C. There is a broad distribution of the plateau force in which three force peaks can be identified by a Gaussian fit (82). These peaks correspond to the unfolding of three types of DNA structures with different stabilities. To further analyze the topology/structure of telomeric DNA based on the unfolding force, we divided the force distribution into three regions according to the most probable value of the three Gaussian peaks: L region (lower force region, 15–40 pN), H region (higher force region, 40–60 pN), and D region (B-S transition of the double helix, 60–75 pN).

The presence of the single-stranded G- and C-chain, as well as the double-stranded DNA caused the appearance of a double-force plateau in the stretching curve. Figure 6A

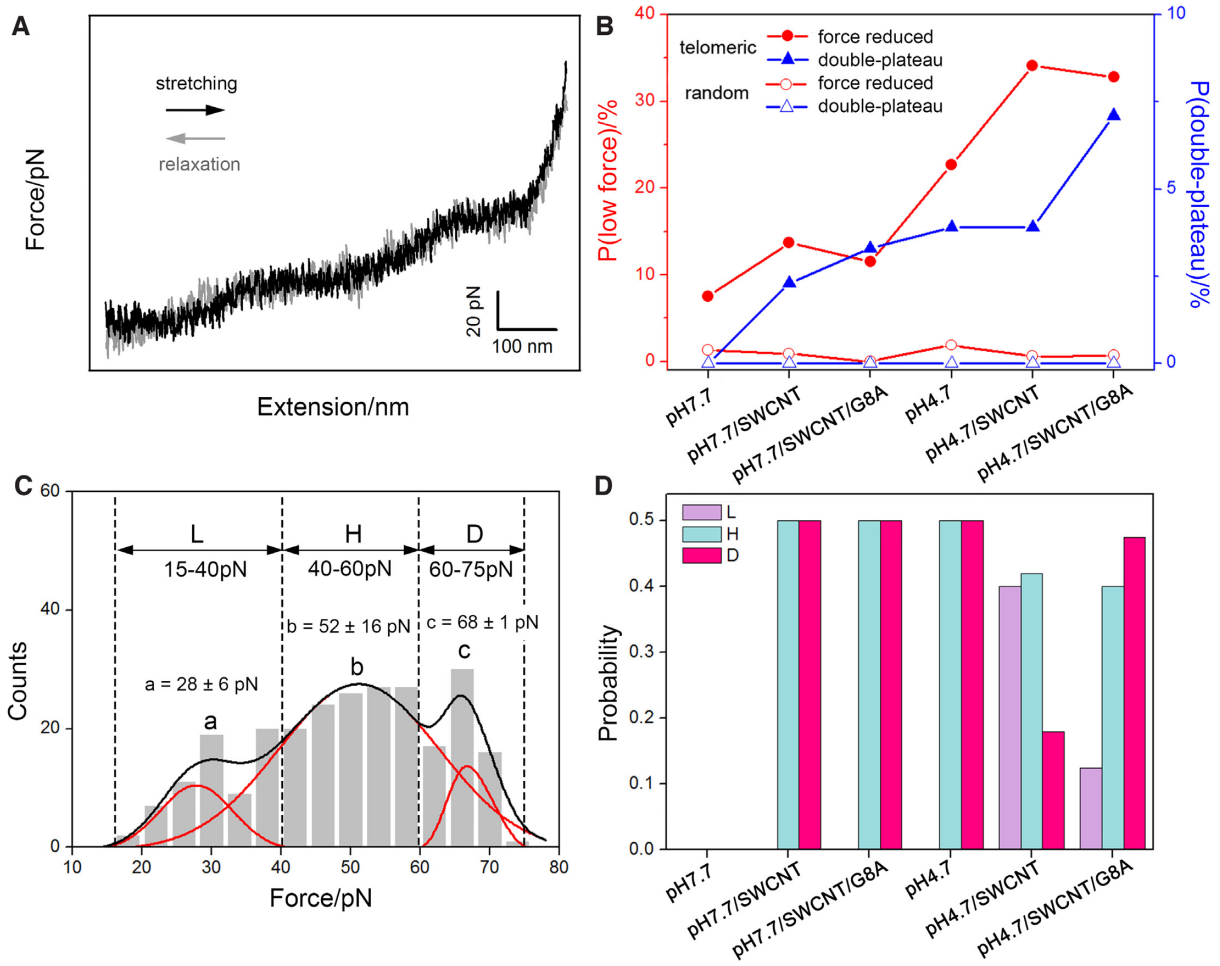

Figure 5. (**A**) Typical stretching (black) and relaxation (gray) curves of telomeric DNA in 10 μg/ml SWCNT-COOH and 100 mM KCl (pH 4.7) at room temperature. (**B**) The probabilities of low-force value plateau (red in circles, left) and double-plateau (blue in triangles, right) in stretching curves in different experimental buffers. The solid and open markers represent telomeric DNA and random DNA, respectively. (**C**) The plateau-force histogram of stretching curves of the double-plateau ($n = 128$). Multiple Gaussian peaks are shown in red with the smoothed curve shown in black. Each Gaussian peak is labeled with a letter (peaks a–c) and the mean force value with standard deviation. (**D**) The proportion of three force regions (L, H, D) in the double-plateau under different experimental conditions.

shows red and blue lines that represent the G-strand and the C-strand, respectively, and a, b, c and d represent the unstructured ssDNA. Here, squared *G* or *C* represent the structures formed by the G-strand or C-strand. These can exist either as a partially folded structure with a lower unfolding force (F_1) or a complete G-quadruplex or i-motif with a higher unfolding force (F_2). When the length of $(a + b)(L(a + b))$ is close to that of $(c + d)$ $(L(c + d))$, the G- and C-strands will be stretched in parallel. F_{unfold} is the sum of F_G and F_C; otherwise, the two strands will be stretched in series. F_{unfold} is the force value of the first unfolding structure.

The 20–30 pN (F_1) may come from the unfolding of some unstable structures like partially folded structures and DNA loops (44,83,84). A further ∼50 pN (F_2) is needed to unfold a G-quadruplex in this experimental condition (85), and the i-motif has a similar stability to G-quadruplex (36). Therefore, we speculate that the L (15–40 pN) region may come from the unfolding of unstable structures and can be partially folded into structures or hairpins. The H (40–60 pN) region may represent the unfolding of complete higher-order structures (G-quadruplexes or i-motifs) in series or a partially folded structure in parallel. Finally, the D (60–75 pN) region should represent the B-S transition of double helix DNA (51) or the unfolding of complete higher-order structure and the partially folded structure in parallel. The unfolding of a complete G-quadruplex and an i-motif in parallel needs about 100 pN, which is close to the rupture force of biotin-streptavidin (∼120 pN), but this is not observed.

The proportions of the three force regions under each condition are shown in Figure 5D. We found that the type of double-plateau has no change after the introduction of G8A in pH 7.7, SWCNT. However, after adding G8A at pH 4.7 with SWCNT and KCl conditions, the probability of L (lower force region) and H (higher force region) decreases, especially L, and the probability of D (B-S transition of the double helix) increases. This may be because the unstable structures on the C-strand like hairpin or loops are destroyed by the renaturation of G8A and C-strand. In

A

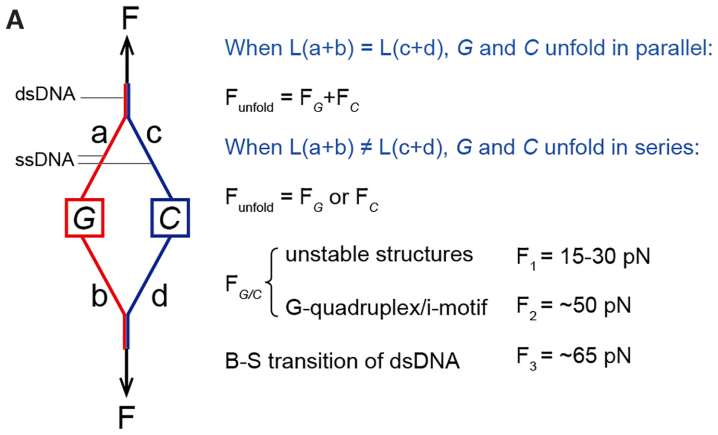

B

region	F(series)	F(parallel)
L 15-40 pN	F_1	F_1+F_1
H 40-60 pN	F_2	F_1+F_1
D 60-75 pN	F_3	F_1+F_2

C

condition	topology
pH 7.7	dsDNA
pH 7.7/SWCNT	dsDNA + GQ/iM
pH 7.7/SWCNT/G8A	dsDNA + GQ/iM
pH 4.7	dsDNA + GQ/iM
pH 4.7/SWCNT	dsDNA + GQ/iM + partially folded structure
pH 4.7/SWCNT/G8A	dsDNA + GQ/iM + partially folded structure

Figure 6. (**A**) Schematic of the dsDNA stretching and corresponding force analysis. (**B**) Possible unfolding force combinations corresponding to the L/H/D regions. (**C**) Major structures under different conditions. GQ and iM represent G-quadruplex and i-motif, respectively.

other words, the addition of G8A can reduce the probability of F_1. Therefore, the H region at pH 7.7 mainly comes from the unfolding of complete higher-order structures (G-quadruplexes or i-motifs) in series ($H = F_2$). At pH 4.7, the H region mainly comes from the unfolding of partially folded structures in parallel ($H = F_1+F_1$). These results indicate that the partially folded structures only form under conditions whereby K^+, acidity, and SWCNT are present. Thus, the probable folding topologies of double-stranded telomeric DNA after force-induced melting under different conditions are summarized in Figure 6C.

The results show that mechanical force is an important factor in inducing DNA topology changes. After the force induction, the final topological structures of telomeric DNA are closely related to the factors that can affect the stability of dsDNA, G-quadruplex and i-motif structures. Figure 7 shows that when telomeric dsDNA is in an environment that can stabilize the double helix, the separated DNA strands can turn back to its original double helical structure after force-induced melting. By gradually increasing the factors of stability reduction of the double helix to the environment, dsDNA renaturation is suppressed, and higher-order structures are easier to form. This can be achieved by reducing the stability of the hydrogen bond (44), including lowering the pH or adding ligands, such as SWCNT, that can stabilize or facilitate the formation of the G-quadruplex or i-motif (39). It should be noted that although the telomeric dsDNA used in the current study is ~700 bp in length, the conformation transition behavior should be similar to the actual behavior of real telomeric dsDNA *in vivo*, since dsDNA will show lower mechanical stability only when the length becomes smaller than ~200 bp (86,87). To further elucidate the effects of repeat length on the structure of telomeric dsDNA, we performed CD experiments on dsDNAs produced by different number of EM-PCR cycles (see Supplementary Figures S11 and S12). Our results show that with the increase of DNA length from 21 bp (0 × Cycle) to 75 bp (5 × Cycle), the stability of dsDNA increases accordingly. For short 21 bp telomeric DNA, the presence of KCl and low pH (4.7) can switch the dsDNA to single-stranded G-quadruplex and i-motif structures (see Supplementary Figure S12A), while the dsDNA becomes the dominate structure for longer (e.g. ~75 bp produced by 5 × Cycle) telomeric dsDNA (Supplementary Figure S12D).

In our current work, we used mechanical force to trigger the strand separation of dsDNA and eventually the formation of G-quadruplexes and i-motifs, and the effective force applied on the DNA is in the range of 30–100 pN. According to previous reports, the force that a single-molecular motor, such as RNA polymerase, can generate is ~15–30

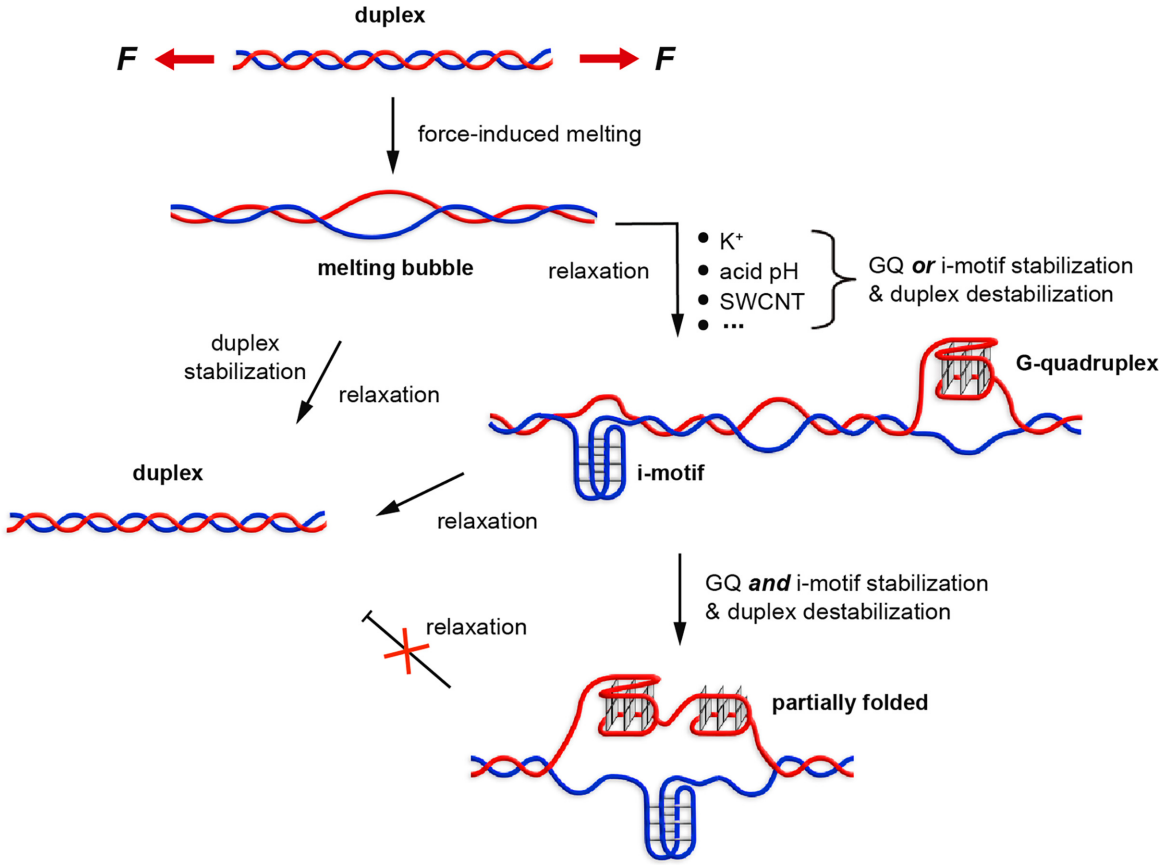

Figure 7. A probable model of telomeric DNA topology after force-induced melting. Different conditions in the renaturation process eventually induce telomeric dsDNA to form different topologies.

pN (88), which is necessary to unzip dsDNA (about 15 pN) (89). In our *in vitro* SMFS experiment, the external forces were applied on the two strands of the dsDNA primarily in a shearing mode. As a result, to separate the two strands, a relatively higher force (e.g. >65 pN) is required. However, *in vivo*, the two strands of the dsDNA can be separated by a molecular motor such as the helicase in the unzipping mode, which requires much lower forces. Although the absolute force values in these two cases are different, the actual results in terms of the strand separation and the formation of G-quadruplexes and i-motifs should be quite similar.

CONCLUSIONS

In this study, we developed an EM-PCR and TA cloning-based method for the preparation of long-chain double-stranded telomeric DNA with a uniform length and modified ends. These are useful for single molecule force spectroscopy studies. We found that mechanical force is an important factor in inducing telomere topology changes. Our results show that the mechanical properties of telomeric DNA are the same as those of normal DNA sequences that undergo a highly cooperative transition at 65 pN. However, telomeric DNA exhibits different mechanical properties from ordinary dsDNA during repeated stretching-relaxation cycles. This can be ascribed to the topology changes of telomeric DNA after force-induced melting. Mechanical force can trigger the separation of the two strands in dsDNA, which allows the formation of higher-order structures (e.g. G-quadruplex or i-motif) during relaxation. The renaturation and separation of G- and C-strands are two competitive dynamic equilibrium processes. Monovalent K^+, acidity, SWCNTs and G8A fragments can shift the equilibrium towards strand separation and promote higher-order structures formation because only the presence of both i-motifs on C-strand and G-quadruplexes on G-strand can suppress the renaturation. Compared with short telomeric strands (e.g. 21 bp), our current system can much accurately observe the actual behavior of double-stranded telomere DNA. The results deepen our understanding of the relevant biological functions of telomeres since mechanical force exists in many biological processes (90). In addition, this method can be used to study other long-chain dsDNA with tandem repeat sequences.

SUPPLEMENTARY DATA

Supplementary Data are available at NAR Online.

ACKNOWLEDGEMENTS

We would like to thank TopEdit (www.topeditsci.com) for English language editing of this manuscript.

FUNDING

National Natural Science Foundation of China [21525418, 21827805]. Funding for open access charge: National Natural Science Foundation of China.
Conflict of interest statement. None declared.

REFERENCES

1. Shay,J.W. and Wright,W.E. (2005) Senescence and immortalization: role of telomeres and telomerase. *Carcinogenesis*, **26**, 867–874.
2. Greider,C.W. (1998) Telomerase activity, cell proliferation, and cancer. *Proc. Natl. Acad. Sci. U.S.A.*, **95**, 90–92.
3. Moyzis,R.K., Buckingham,J.M., Cram,L.S., Dani,M., Deaven,L.L., Jones,M.D., Meyne,J., Ratliff,R.L. and Wu,J.R. (1988) A highly conserved repetitive DNA sequence, $(TTAGGG)_n$, present at the telomeres of human chromosomes. *Proc. Natl. Acad. Sci. U.S.A.*, **85**, 6622–6626.
4. Morin,G.B. (1989) The human telomere teriminal transferase enzyme is a ribonucleoprotein that synthesizes TTAGGG repeats. *Cell*, **59**, 521–529.
5. McElligott,R. and Wellinger,R.J. (1997) The terminal DNA structure of mammalian chromosomes. *EMBO J.*, **16**, 3705–3714.
6. Wright,W.E., Tesmer,V.M., Huffman,K.E., Levene,S.D. and Shay,J.W. (1997) Normal human chromosomes have long G-rich telomeric overhangs at one end. *Gene. Dev.*, **11**, 2801–2809.
7. Griffith,J.D., Comeau,L., Rosenfield,S., Stansel,R.M., Bianchi,A., Moss,H. and de Lange,T. (1999) Mammalian telomeres end in a large duplex loop. *Cell*, **97**, 503–514.
8. de Lange,T. (2004) T-loops and the origin of telomeres. *Nat. Rev. Mol. Cell. Bio.*, **5**, 323–329.
9. de Lange,T. (2009) How telomeres solve the end-protection problem. *Science*, **326**, 948–952.
10. Biffi,G., Tannahill,D., McCafferty,J. and Balasubramanian,S. (2013) Quantitative visualization of DNA G-quadruplex structures in human cells. *Nat. Chem.*, **5**, 182–186.
11. Sun,D., Thompson,B., Cathers,B.E., Salazar,M., Kerwin,S.M., Trent,J.O., Jenkins,T.C., Neidle,S. and Hurley,L.H. (1997) Inhibition of human telomerase by a G-quadruplex-interactive compound. *J. Med. Chem.*, **40**, 2113–2116.
12. Chen,C., Wang,Q., Liu,J., Hao,Y. and Tan,Z. (2011) Contribution of telomere G-quadruplex stabilization to the inhibition of telomerase-mediated telomere extension by chemical ligands. *J. Am. Chem. Soc.*, **133**, 15036–15044.
13. Moye,A.L., Porter,K.C., Cohen,S.B., Phan,T., Zyne,K.G., Sasaki,N., Lovrecz,G.O., Beck,J.L. and Bryan,T.M. (2015) Telomeric G-quadruplexes are a substrate and site of localization for human telomerase. *Nat. Commun.*, **6**, 7643.
14. Rhodes,D. and Lipps,H.J. (2015) G-quadruplexes and their regulatory roles in biology. *Nucleic Acids Res.*, **43**, 8627–8637.
15. Hänsel-Hertsch,R., Antonio,M.D. and Balasubramanian,S. (2017) DNA G-quadruplexes in the human genome: detection, functions and therapeutic potential. *Nat. Rev. Mol. Cell. Biol.*, **18**, 279–284.
16. Hillen,H.S., Parshin,A.V., Agaronyan,K., Morozov,Y.I., Graber,J.J., Chernev,A., Schwinghammer,K., Urlaub,H., Anikin,M., Cramer,P. *et al.* (2017) Mechanism of transcription anti-termination in human mitochondria. *Cell*, **171**, 1082–1093.
17. Leroy,J.L., Gueron,M., Mergny,J.L. and Helene,C. (1994) Intramolecular folding of a fragment of the cytosine-rich strand of telomeric DNA into an i-motif. *Nucleic Acids Res.*, **22**, 1600–1606.
18. Diederichsen,U. (1998) Oligomers with intercalating cytosine-cyosine$^+$ base pairs and peptide backone: DNA i-motif analogues. *Angew. Chem. Int. Ed.*, **37**, 2273–2276.
19. Zeraati,M., Langley,D.B., Schofield,P., Moye,A.L., Rouet,R., Hughes,W.E., Bryan,T.M., Dinger,M.E. and Christ,D. (2018) I-motif DNA structures are formed in the nuclei of human cells. *Nat. Chem.*, **10**, 631–637.
20. Day,H.A., Pavlou,P. and Waller,Z.A. (2014) I-motif DNA: structure, stability and targeting with ligands. *Bioorg. Med. Chem.*, **22**, 4407–4418.
21. Rajendran,A., Nakanoab,S. and Sugimoto,N. (2010) Molecular crowding of the cosolutes induces an intramolecular i-motif structure of triplet repeat DNA oligomers at neutral pH. *Chem. Commun.*, **46**, 1299–1301.
22. Cui,J., Waltman,P., Le,V.H. and Lewis,E.A. (2013) The effect of molecular crowding on the stability of human c-MYC promoter sequence i-motif at neutral pH. *Molecules*, **18**, 12751–12767.
23. Sun,D. and Hurley,L.H. (2009) The importance of negative superhelicity in inducing the formation of G-quadruplex and i-motif structures in the c-MYC promoter: Implications for drug targeting and control of gene expression. *J. Med. Chem.*, **52**, 2863–2874.
24. Phan,A.T., Guéron,M. and Leroy,J.L. (2000) The solution structure and internal motions of a fragment of the cytidine-rich strand of the human telomere. *J. Mol. Biol.*, **299**, 123–144.
25. Brooks,T.A., Kendrick,S. and Hurley,L. (2010) Making sense of G-quadruplex and i-motif functions in oncogene promoters. *FEBS J.*, **277**, 3459–3469.
26. Kang,H.J., Kendrick,S., Hecht,S.M. and Hurley,L.H. (2014) The transcriptional complex between the BCL2 i-motif and hnRNP LL is a molecular switch for control of gene expression that can be modulated by small molecules. *J. Am. Chem. Soc.*, **136**, 4172–4185.
27. Kendrick,S., Kang,H.J., Alam,M.P., Madathil,M.M., Agrawal,P., Gokhale,V., Yang,D., Hecht,S.M. and Hurley,L.H. (2014) The dynamic character of the BCL2 promoter i-motif provides a mechanism for modulation of gene expression by compounds that bind selectively to the alternative DNA hairpin structure. *J. Am. Chem. Soc.*, **136**, 4161–4171.
28. Sutherland,C., Cui,Y., Mao,H. and Hurley,L.H. (2016) A mechanosensor mechanism controls the G-quadruplex/i-motif molecular switch in the *MYC* promoter NHE III_1. *J. Am. Chem. Soc.*, **138**, 14138–14151.
29. Brown,R.V., Wang,T., Chappeta,V.R., Wu,G., Onel,B., Chawla,R., Quijada,H., Camp,S.M., Chiang,E.T., Lassiter,Q.R. *et al.* (2017) The consequences of overlapping G-quadruplexes and i-motifs in the platelet-derived growth factor receptor β; core promoter nuclease hypersensitive element can explain the unexpected effects of mutations and provide opportunities for selective targeting of both structures by small molecules to downregulate gene expression. *J. Am. Chem. Soc.*, **139**, 7456–7475.
30. Kaiser,C.E., Ert,N.A.V., Agrawal,P., Chawla,R., Yang,D. and Hurley,L.H. (2017) Insight into the complexity of the i-motif and G-quadruplex DNA structures formed in the *KRAS* promoter and subsequent drug-induced gene repression. *J. Am. Chem. Soc.*, **139**, 8522–8536.
31. Takahashia,S., Brazierb,J.A. and Sugimoto,N. (2017) Topological impact of noncanonical DNA structures on Klenow fragment of DNA polymerase. *Proc. Natl. Acad. Sci. U.S.A.*, **114**, 9605–9610.
32. Miura,T. and Thomas,J.G. Jr (1994) Structural polymorphism of telomere DNA: Interquadruplex and duplex-quadruplex conversions probed by Raman spectroscopy. *Biochemistry*, **33**, 7848–7856.
33. Deng,H. and Braunlin,W.H. (1995) Duplex to quadruplex equilibrium of the self-complementary oligonucleotide d(GGGGCCCC). *Biopolymers*, **35**, 677–681.
34. Li,W., Wu,P., Ohmichi,T. and Sugimoto,N. (2002) Characterization and thermodynamic properties of quadruplex/duplex competition. *FEBS Lett.*, **526**, 77–81.
35. Phan,A.T. and Mergny,J.L. (2002) Human telomeric DNA: G-quadruplex, i-motif and watson-crick double helix. *Nucleic Acids Res.*, **30**, 4618–4625.
36. Dhakal,S., Yu,Z., Konik,R., Cui,Y., Koirala,D. and Mao,H. (2012) G-quadruplex and i-motif are mutually exclusive in ILPR double-stranded DNA. *Biophys. J.*, **102**, 2575–2584.
37. Assi,H.A., El-Khoury,R., Gonzalez,C. and Damha,M.J. (2017) 2′-Fluoroarabinonucleic acid modification traps G-quadruplex and i-motif structures in human telomeric DNA. *Nucleic Acids Res.*, **45**, 11535–11546.
38. Miyoshi,D., Matsumura,S., Nakano,S. and Sugimoto,N. (2004) Duplex dissociation of telomere DNAs induced by molecular crowding. *J. Am. Chem. Soc.*, **126**, 165–169.
39. Li,X., Peng,Y., Ren,J. and Qu,X. (2006) Carboxyl-modified single-walled carbon nanotubes selectively induce human telomeric i-motif formation. *Proc. Natl. Acad. Sci. U.S.A.*, **103**, 19658–19663.
40. Guo,K., Pourpak,A., Beetz Rogers,K., Gokhale,V., Sun,D. and Hurley,L.H. (2007) Formation of pseudosymmetrical G-quadruplex and i-motif structures in the proximal promoter region of the *RET* oncogene. *J. Am. Chem. Soc.*, **129**, 10220–10228.

41. Endo,M., Xing,X., Zhou,X., Emura,T., Hidaka,K., Tuesuwan,B. and Sugiyama,H. (2015) Single-molecule manipulation of the duplex formation and dissociation at the G-quadruplex/i-motif site in the DNA nanostructure. *ACS Nano*, **9**, 9922–9929.
42. Cui,Y., Kong,D., Ghimire,C., Xu,C. and Mao,H. (2016) Mutually exclusive formation of G-quadruplex and i-motif is a general phenomenon governed by steric hindrance in duplex DNA. *Biochemistry*, **55**, 2291–2299.
43. Panczyk,T. and Wolski,P. (2018) Molecular dynamics analysis of stabilities of the telomeric Watson-Crick duplex and the associated i-motif as a function of pH and temperature. *Biophys. Chem.*, **237**, 22–30.
44. Wolski,P., Nieszporek,K. and Panczyk,T. (2019) G-quadruplex and i-motif structures within the telomeric DNA duplex. A molecular dynamics analysis of protonation states as factors affecting their stability. *J. Phys. Chem. B*, **123**, 468–479.
45. Selvam,S., Koirala,D., Yu,Z. and Mao,H. (2014) Quantification of topological coupling between DNA superhelicity and G-quadruplex formation. *J. Am. Chem. Soc.*, **136**, 13967–13970.
46. Hoffman,B.D., Grashoff,C. and Schwartz,M.A. (2011) Dynamic molecular processes mediate cellular mechanotransduction. *Nature*, **475**, 316–323.
47. Krieg,M., Fläschner,G., Alsteens,D., Gaub,B.M., Roos,W.H., Wuite,G.J.L., Gaub,H.E., Gerber,C., Dufrêne,Y.F. and Müller,D.J. (2018) Atomic force microscopy-based mechanobiology. *Nat. Rev. Phys.*, **1**, 41–57.
48. Burridge,K., Monaghan-Benson,E. and Graham,D.M. (2019) Mechanotransduction: from the cell surface to the nucleus via RhoA. *Philos. T. R. Soc. B*, **374**, 20180229.
49. Sankaran,J., Uzer,G., van Wijnen,A.J. and Rubin,J. (2019) Gene regulation through dynamic actin control of nuclear structure. *Exp. Biol. Med.*, **244**, 1345–1353.
50. Smith,S.B., Cui,Y. and Bustamante,C. (1996) Overstretching B-DNA: The Elastic Response of Individual Double-Stranded and Single-Stranded DNA Molecules. *Science*, **271**, 795–799.
51. Paik,D.H. and Perkins,T.T. (2011) Overstretching DNA at 65 pN does not require peeling from free ends or nicks. *J. Am. Chem. Soc.*, **133**, 3219–3221.
52. Burmistrova,A., Fresch,B., Sluysmans,D., Pauw,E.D., Remacle,F. and Duwez,A.-S. (2016) Force measurements reveal how small binders perturb the dissociation mechanisms of DNA duplex sequences. *Nanoscale*, **8**, 11718–11726.
53. Kilchherr,F., Wachauf,C., Pelz,B., Rief,M., Zacharias,M. and Dietz,H. (2016) Single-molecule dissection of stacking forces in DNA. *Science*, **353**, 5508.
54. Schlotterer,C. and Tautz,D. (1992) Slippage synthesis of simple sequence DNA. *Nucleic Acids Res.*, **20**, 211–215.
55. Petruska,J., Hartenstine,M.J. and Goodman,M.F. (1998) Analysis of strand slippage in DNA polymerase expansions of CAG/CTG triplet repeats associated with neurodegenerative disease. *J. Biol. Chem.*, **273**, 5204–5210.
56. Hartenstine,M.J., Goodman,M.F. and Petruska,J. (2000) Base stacking and even/odd behavior of hairpin loops in DNA triplet repeat slippage and expansion with DNA polymerase. *J. Biol. Chem.*, **275**, 18382–18390.
57. Whitfield,C.J., Turley,A.T., Tuite,E.M., Connolly,B.A. and Pike,A.R. (2015) Enzymatic method for the synthesis of long DNA sequences with multiple repeat units. *Angew. Chem. Int. Ed.*, **54**, 8971–8974.
58. Raeymaekers,L. (1995) A commentary on the practical applications of competitive PCR. *Genome Res.*, **5**, 91–94.
59. Rief,M., Clausen-Schaumann,H. and Gaub,H.E. (1999) Sequence-dependent mechanics of single DNA molecules. *Nat. Struct. Biol.*, **6**, 346–349.
60. Zhang,X., Chen,H., Le,S., Rouzina,I., Doylea,P.S. and Yan,J. (2013) Revealing the competition between peeled ssDNA, melting bubbles, and S-DNA during DNA overstretching by single-molecule calorimetry. *Proc. Natl. Acad. Sci. U.S.A.*, **110**, 3865–3870.
61. Punnoose,J.A., Cui,Y., Koirala,D., Yangyuoru,P.M., Ghimire,C., Shrestha,P. and Mao,H. (2014) Interaction of G-quadruplexes in the full-length 3′ human telomeric overhang. *J. Am. Chem. Soc.*, **136**, 18062–18069.
62. You,H., Wu,J., Shao,F. and Yan,J. (2015) Stability and kinetics of c-MYC promoter G-quadruplexes studied by single-molecule manipulation. *J. Am. Chem. Soc.*, **137**, 2424–2427.
63. Shrestha,P., Jonchhe,S., Emura,T., Hidaka,K., Endo,M., Sugiyama,H. and Mao,H. (2017) Confined space facilitates G-quadruplex formation. *Nat. Nanotechnol.*, **12**, 582–588.
64. Liu,K., Song,Y., Feng,W., Liu,N., Zhang,W. and Zhang,X. (2011) Extracting a single polyethylene oxide chain from a single crystal by a combination of atomic force microscopy imaging and single-molecule force spectroscopy: Toward the investigation of molecular interactions in their condensed states. *J. Am. Chem. Soc.*, **133**, 3226–3229.
65. Xue,Y., Li,X., Li,H. and Zhang,W. (2014) Quantifying thiol-gold interactions towards the efficient strength control. *Nat. Commun.*, **5**, 4348.
66. Chen,Y., Ma,K., Hu,T., Jiang,B., Xu,B., Tian,W., Sun,J.Z. and Zhang,W. (2015) Investigation of the binding modes between AIE-active molecules and dsDNA by single molecule force spectroscopy. *Nanoscale*, **7**, 8939–8945.
67. Li,Z., Song,Y., Li,A., Xu,W. and Zhang,W. (2018) Direct observation of the wrapping/unwrapping of ssDNA around/from a SWCNT at the single-molecule level: towards tuning the binding mode and strength. *Nanoscale*, **10**, 18586–18596.
68. Song,Y., Ma,Z., Yang,P., Zhang,X., Lyu,X., Jiang,K. and Zhang,W. (2019) Single-molecule force spectroscopy study on force-induced melting in polymer single crystals: The chain conformation matters. *Macromolecules*, **52**, 1327–1333.
69. Cluzel,P., Lebrun,A., Heller,C., Lavery,R., Viovy,J.-L., Chatenay,D. and Caron,F. (1996) DNA: An extensible molecule. *Science*, **271**, 792–794.
70. Zhang,X., Chen,H., Fu,H., Doyle,P.S. and Yan,J. (2012) Two distinct overstretched DNA structures revealed by single-molecule thermodynamics measurements. *Proc. Natl. Acad. Sci. U.S.A.*, **109**, 8103–8108.
71. Zhang,X., Chen,H., Le,S., Rouzina,I., Doyle,P.S. and Yan,J. (2013) Revealing the competition between peeled ssDNA, melting bubbles, and S-DNA during DNA overstretching by single-molecule calorimetry. *Proc. Natl. Acad. Sci. U.S.A.*, **110**, 3865–3870.
72. Fu,H., Chen,H., Marko,J.F. and Yan,J. (2010) Two distinct overstretched DNA states. *Nucleic Acids Res.*, **38**, 5594–5600.
73. Fu,H., Chen,H., Zhang,X., Qu,Y., Marko,J.F. and Yan,J. (2011) Transition dynamics and selection of the distinct S-DNA and strand unpeeling modes of double helix overstretching. *Nucleic Acids Res.*, **39**, 3473–3481.
74. Bethea,D., Fullmer,B., Syed,S., Seltzer,G., Tiano,J., Rischko,C., Gillespie,L., Brown,D. and Gasparro,F.P. (1999) Psoralen photobiology and photochemotherapy: 50 years of science and medicine. *J. Dermatol. Sci.*, **19**, 78–88.
75. Pearlman,D.A., Holbrook,S.R., Pirkle,D.H. and Kim,S.H. (1985) Molecular models for DNA damaged by photoreaction. *Science*, **227**, 1304–1308.
76. Cocco,S., Yan,J., Leger,J.F., Chatenay,D. and Marko,J.F. (2004) Overstretching and force-driven strand separation of double-helix DNA. *Phys. Rev. E*, **70**, 011910.
77. King,G.A., Gross,P., Bockelmann,U., Modesti,M., Wuite,G.J.L. and Peterman,E.J.G. (2013) Revealing the competition between peeled ssDNA, melting bubbles, and S-DNA during DNA overstretching using fluorescence microscopy. *Proc. Natl. Acad. Sci. U.S.A.*, **110**, 3859–3864.
78. Chen,Y., Qu,K., Zhao,C., Wu,L., Ren,J., Wang,J. and Qu,X. (2012) Insights into the biomedical effects of carboxylated single-wall carbon nanotubes on telomerase and telomeres. *Nat. Commun.*, **3**, 1074.
79. Caterino,M., D'Aria,F., Kustov,A.V., Belykh,D.V., Khudyaeva,I.S., Starseva,O.M., Berezin,D.B., Pylina,Y.I., Usacheva,T., Amato,J. and Giancola,C. (2020) Selective binding of a bioactive porphyrin-based photosensitizer to the G-quadruplex from the KRAS oncogene promoter. *Int. J. Biol. Macromol.*, **145**, 244–251.
80. Khan,S.J., Yanez,G., Seldeen,K., Wang,H., Lindsay,S.M. and Fletcher,T.M. (2007) Interactions of TRF2 with model telomeric ends. *Biochem. Biophys. Res. Commun.*, **363**, 44–50.
81. Pedroso,I.M., Hayward,W. and Fletcher,T.M. (2009) The effect of the TRF2 N-terminal and TRFH regions on telomeric G-quadruplex structures. *Nucleic Acids Res.*, **37**, 1541–1554.
82. Kar,A., Jones,N., Arat,N.O., Fishel,R. and Griffith,J. (2018) Long repeating (TTAGGG)n single stranded DNA self-condenses into compact beaded filaments stabilized by G-quadruplex formation. *J. Biol. Chem.*, **24**, 9473–9485.

83. Dhakal,S., Schonhoft,J.D., Koirala,D., Yu,Z., Basu,S. and Mao,H. (2010) Coexistence of an ILPR i-motif and a partially folded structure with comparable mechanical stability revealed at the single-molecule level. *J. Am. Chem. Soc.*, **132**, 8991–8997.
84. Tran,P.L., Mergny,J.L. and Alberti,P. (2011) Stability of telomeric G-quadruplexes. *Nucleic Acids Res.*, **39**, 3282–3294.
85. Lynch,S., Baker,H., Byker,S.G., Zhou,D. and Sinniah,K. (2009) Single molecule force spectroscopy on G-quadruplex DNA. *Chem. Eur. J.*, **15**, 8113–8116.
86. Zhang,W., Barbagallo,R., Madden,C., Roberts,C.J., Woolford,A. and Allen,S. (2005) Progressing single biomolecule force spectroscopy measurements for the screening of DNA binding agents. *Nanotechnology*, **16**, 2325–2333.
87. Zoli,M. (2016) Flexibility of short DNA helices under mechanical stretching. *Phys. Chem. Chem. Phys.*, **18**, 17666–17677.
88. Wang,M.D., Schnitzer,M.J., Yin,H., Landick,R., Gelles,J. and Block,S.M. (1998) Force and velocity measured for single molecules of RNA polymerase. *Science*, **282**, 902–907.
89. Essevaz-Roulet,B., Bockelmann,U. and Heslot,F. (1997) Mechanical separation of the complementary strands of DNA. *Proc. Natl. Acad. Sci. U.S.A.*, **94**, 11935–11940.
90. Freikamp,A., Mehlich,A., Klingner,C. and Grashoff,C. (2017) Investigating piconewton forces in cells by FRET-based molecular force microscopy. *J. Struct. Biol.*, **197**, 37–42.